Supplement of

Earth's future climate and its variability simulated at 9 km global resolution

Ja-Yeon Moon[1,2], Jan Streffing[3], Sun-Seon Lee[1,2], Tido Semmler[3,4], Miguel Andrés-Martínez[3], Jiao Chen[3], Eun-Byeoul Cho[1,2], Jung-Eun Chu[5], Christian Franzke[1,6], Jan P. Gärtner[3], Rohit Ghosh[3], Jan Hegewald[3,7], Songyee Hong[8], Nikolay Koldunov[3], June-Yi Lee[1,6], Zihao Lin[5], Chao Liu[9], Svetlana Loza[3], Wonsun Park[1,6], Woncheol Roh[1,2], Dmitry V. Sein[3,10], Sahil Sharma[1,2], Dmitry Sidorenko[3], Jun-Hyeok Son[1,2], Malte F. Stuecker[11], Qiang Wang[3], Gyuseok Yi[1,6], Martina Zapponini[3], Thomas Jung[3,12*], Axel Timmermann[1,2*]

[1]IBS Center for Climate Physics, Busan, 46241, Republic of Korea
[2]Pusan National University, Busan, 46241, Republic of Korea
[3]Alfred Wegener Institute, Helmholtz Centre for Polar and Marine Research, Bremerhaven, 27570, Germany
[4]Met Éireann, 65-67 Glasnevin Hill, D09 Y921, Dublin, Ireland
[5]Low-Carbon and Climate Impact Research Centre, School of Energy and Environment, City University of Hong Kong, Hong Kong, China
[6]Department of Climate System, Pusan National University, Busan, 46241, Republic of Korea
[7]Gauß-IT-Zentrum, Braunschweig University of Technology (GITZ), Braunschweig, Germany
[8]SSG services, Lenovo, Seoul, 06141, Republic of Korea
[9]Irreversible Climate Change Research Center, Yonsei University, Seoul, 03722, Republic of Korea
[10]Shirshov Institute of Oceanology, Russian Academy of Science, Moscow 117997, Russia
[11]Department of Oceanography and International Pacific Research Center, University of Hawai'i at Mānoa, Honolulu, 96822, USA
[12]Department of Physics and Electrical Engineering, University of Bremen, 28359, Bremen, Germany

Correspondence to: Thomas Jung (Thomas.Jung@awi.de) and Axel Timmermann (axel@ibsclimate.org)

Contents of this file

- Method for Okubo-Weiss-Zeta Parameter with equations (S1-S2)
- Table S1
- Figures S1 to S10

Equations (S1-S2):

The OWZP is a resolution independent tracking method to detect tropical cyclones (Tory et al., 2013a, b). It primarily relies on Okubo-Weiss Parameter and other large-scale variables that are interpolated to 1°×1° grid. Here we provide a brief introduction to the OWZP tracking scheme. The detailed algorithm is explained in the references.

The Okubo-Weiss Parameter is a measure of the low-deformation vorticity

$$OW = \xi^2 - (E^2 + F^2) \quad \text{(S1)}$$

where $E = \left(\frac{\partial u}{\partial x}\right) - \left(\frac{\partial v}{\partial y}\right)$ and $F = \left(\frac{\partial v}{\partial x}\right) + \left(\frac{\partial u}{\partial y}\right)$ are the square of the stretching and shearing deformation, respectively. Then, Okubo-Weiss-Zeta parameter is calculated by calculating vertical component of absolute vorticity ($\eta = \xi + f$) weighted by $OW_{norm} = [\xi^2 - (E^2 + F^2)]/\xi^2$ and multiplied by the sign of Coriolis parameter f for a consistent cyclonic vorticity in both hemispheres:

$$OWZ = \eta \times (OW_{norm}, 0) \times sign(f) \quad \text{(S2)}$$

Therefore, OWZ and absolute vorticity have a similar magnitude, and the OWZ to η ratio gets smaller when the flow has strong deformation.

The potential to support TC formations is identified by the “initial” thresholds (Table SX) for OWZ at 850 hPa and 500 hPa, relative humidity at 950 hPa and 700 hPa, vertical wind shear between 850 hPa and 200 hPa, and specific humidity at 950 hPa. The threshold values were obtained from Raavi et al. (2023).

Neighboring grid points that meet the initial thresholds are merged together and create a single “clump”, representing a storm at a specific time. Weaker and smaller in close proximity are eliminated. The identified clumps are then tracked forward in time until no clumps remain. At each position along the storm track, the storm is assigned individual values for OWZ, relative humidity, vertical wind shear, and specific humidity. If the updated values pass the “core” threshold (Table S1), it is labeled as “true”. If a sequence of clumps meets consecutive “true” labels for 48 h or more, the storm is considered as a tropical cyclone. In our study, we utilized 6 hourly data, therefore, the criteria for identifying a tropical cyclone is based on the presence of nine consecutive “true” clumps along the track, with the ninth “true” position being designated as the location of storm genesis.

Table S1: Initial and core thresholds for tracking tropical cyclones (TCs) using Okubo–Weiss–Zeta parameter (OWZP) detection scheme.

Criterion	OWZ_{850}	OWZ_{500}	RH_{950}	RH_{700}	$VWS_{850\text{-}200}$	SH_{950}
Initial	$> 50\times10^{-6}$ s^{-1}	$> 40\times10^{-6}$ s^{-1}	> 70 %	> 50%	< 25 m s^{-1}	>10 g kg^{-1}
Core	$> 60\times10^{-6}$ s^{-1}	$> 50\times10^{-6}$ s^{-1}	> 85 %	> 70%	< 12.5 m s^{-1}	>14 g kg^{-1}

Figures S1 to S9:

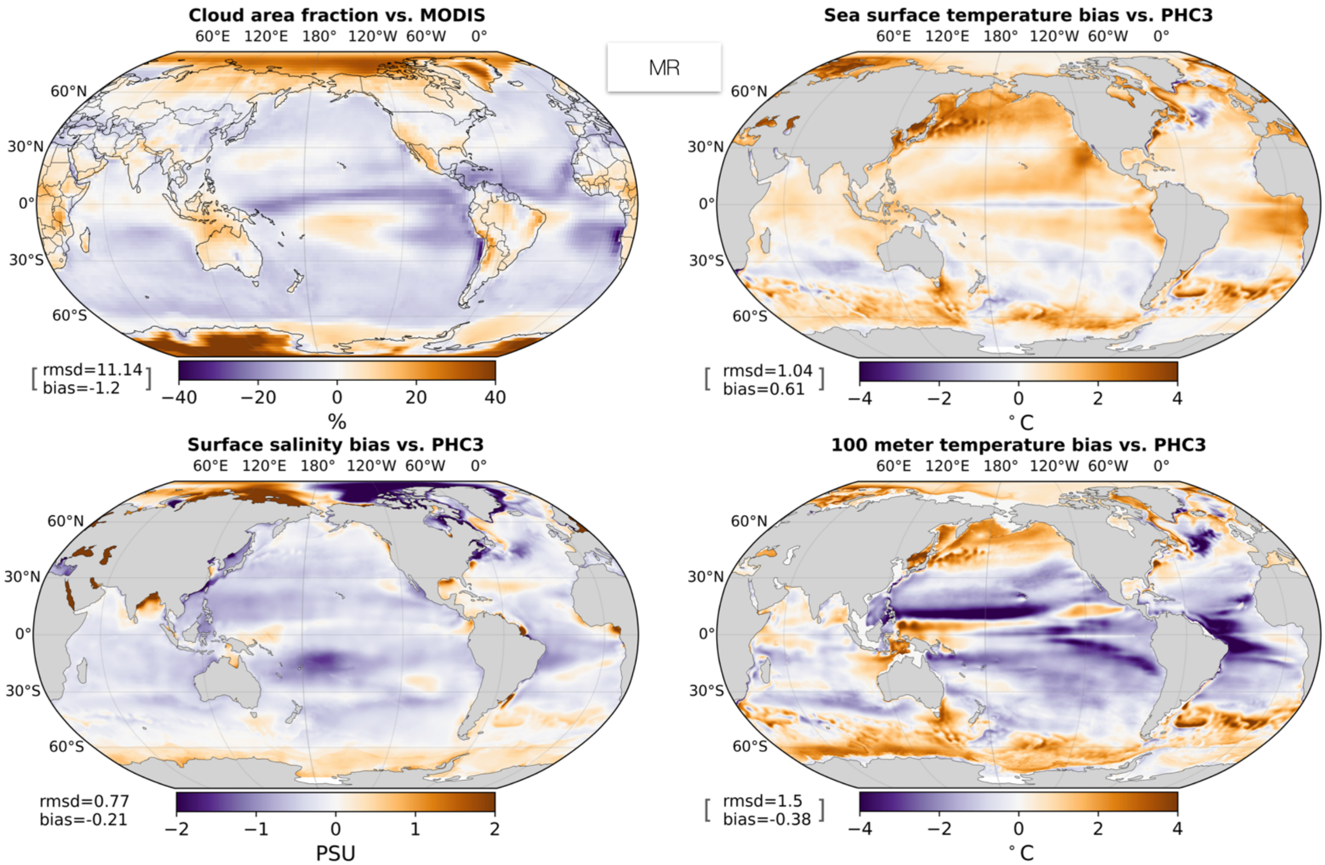

Figure S1: Bias of simulated total cloudiness in AWI-CM3 MR historical (2002-2012) simulation (upper left) relative to MODIS cloud product (2000-2011) (Kato et al., 2018). Other panels: bias maps for sea surface temperature, sea surface salinity and 100 m temperature relative to the observational PHC climatology (1900-1997) (Steele et al., 2001).

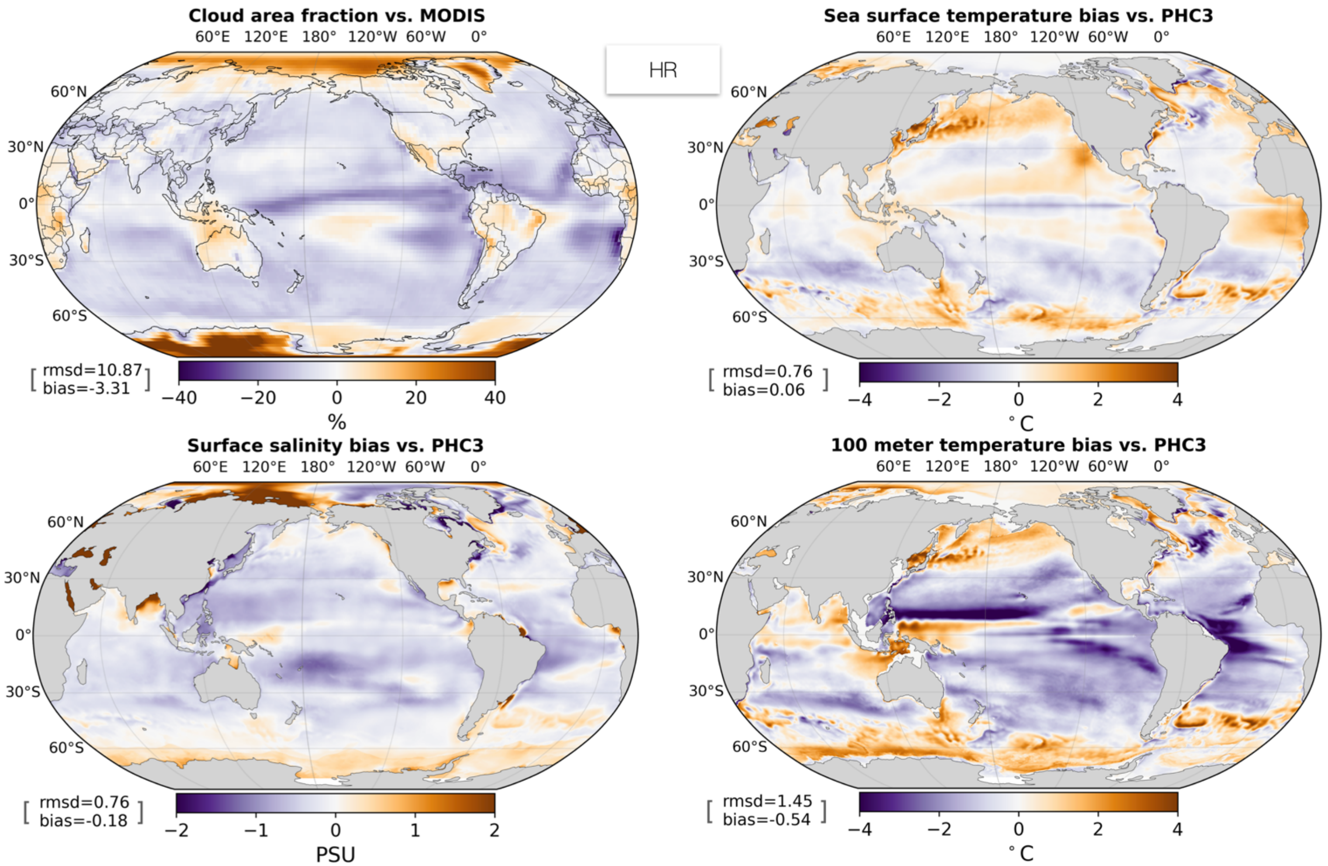

Figure S2: Bias of simulated total cloudiness in AWI-CM3 HR 2000s (2002-2012) snapshot simulation (upper left) relative to MODIS cloud product (2000-2011) (Kato et al., 2018). Other panels: bias maps for sea surface temperature, sea surface salinity and 100 m temperature relative to the observational PHC climatology (Steele et al., 2001).

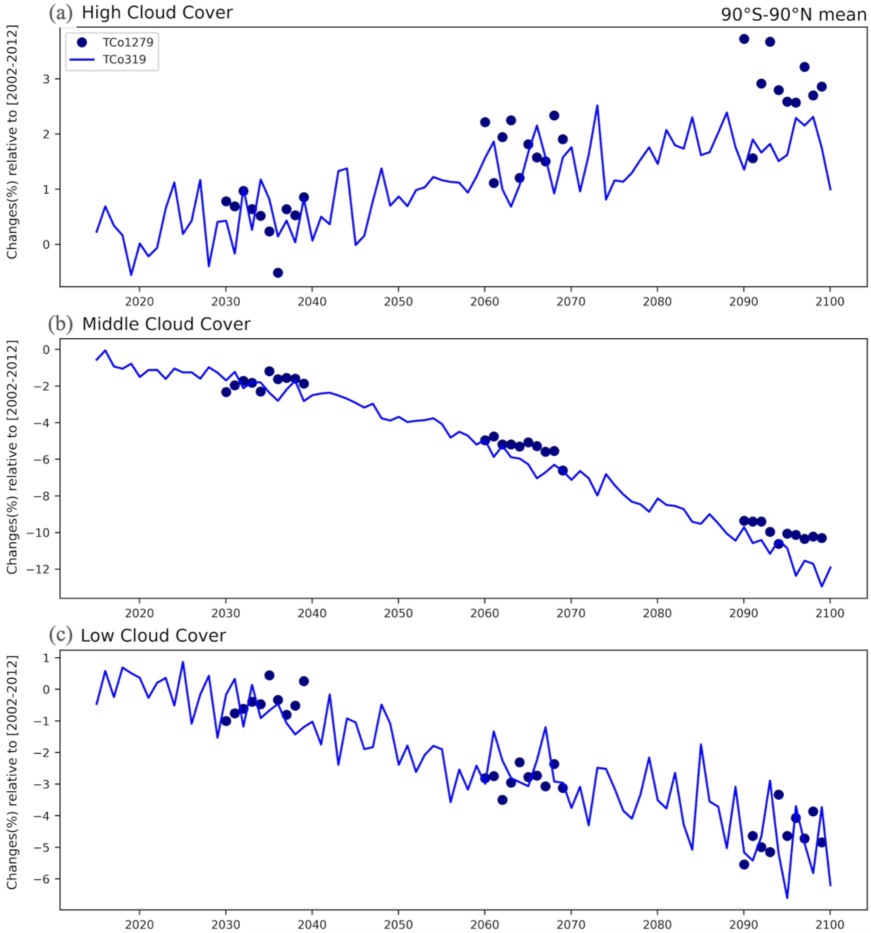

Figure S3: Annual mean difference of global mean (a) high, (b) middle, (c) low cloud cover in MR simulation (blue line) and HR (navy dot) snapshot simulations relative to 2000s.

.

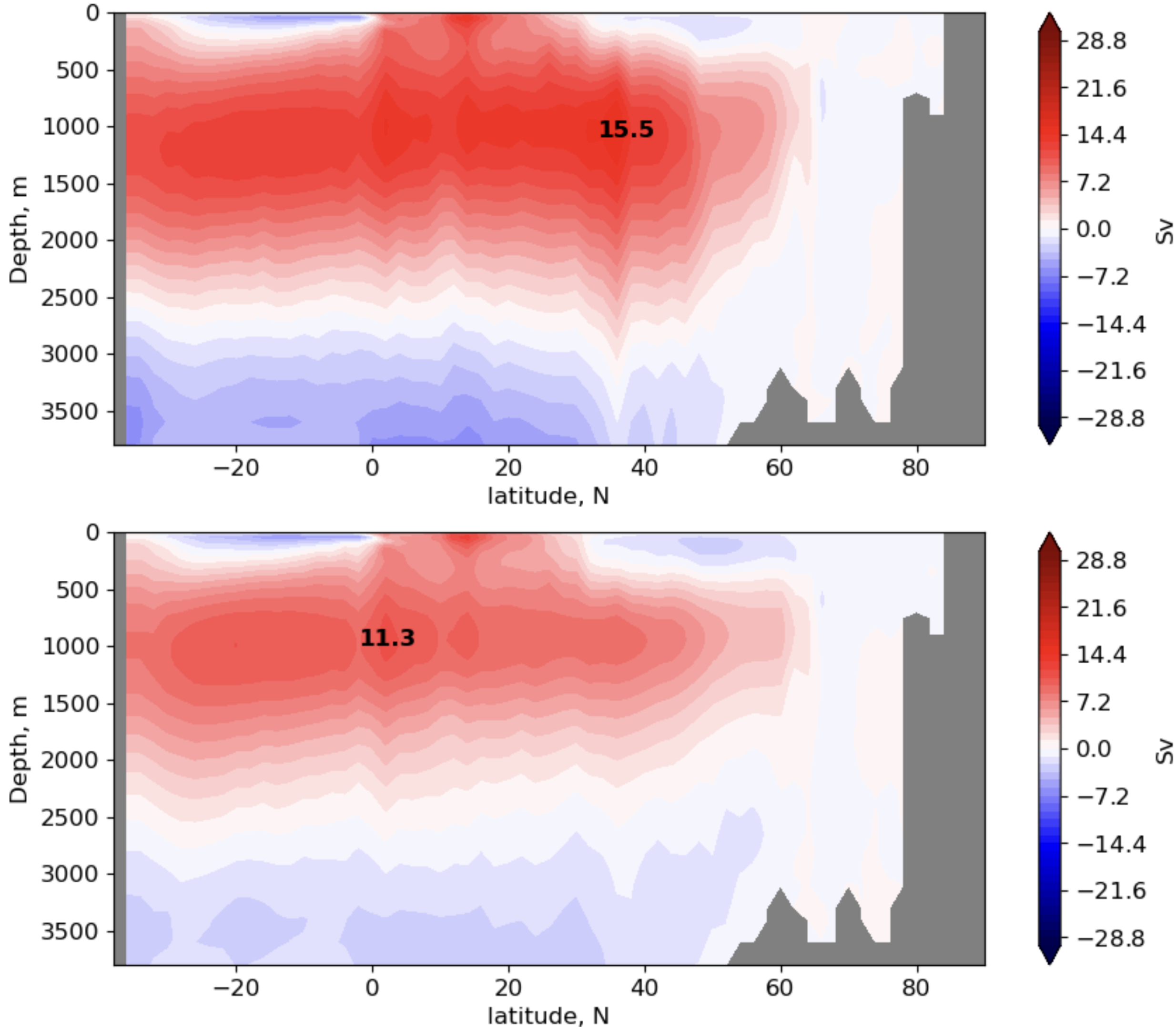

Figure S4: Atlantic Meridional Streamfunction [Sv] for HR simulation, upper: average for years 2000-2009; lower: average for years 2090-2099. The number indicates the maximum value of the streamfunction in the northern Hemisphere.

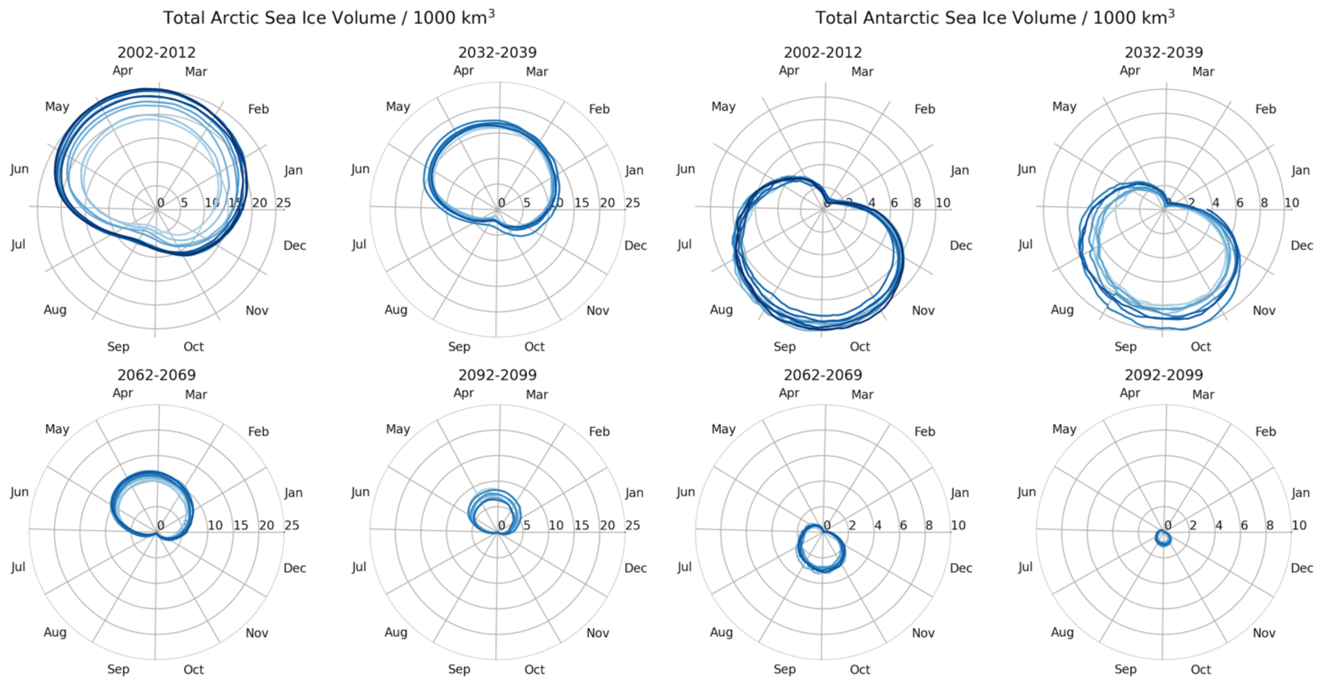

Figure S5: Seasonal cycle of sea-ice volume in Arctic Ocean (left) and Southern Ocean (right) for 2000s and 2030s HR snapshot simulations. Unit [1000 km^3]. The sea ice amplitude in the phase-wheel diagram is represented by the radius and the seasonal phase by the angle.

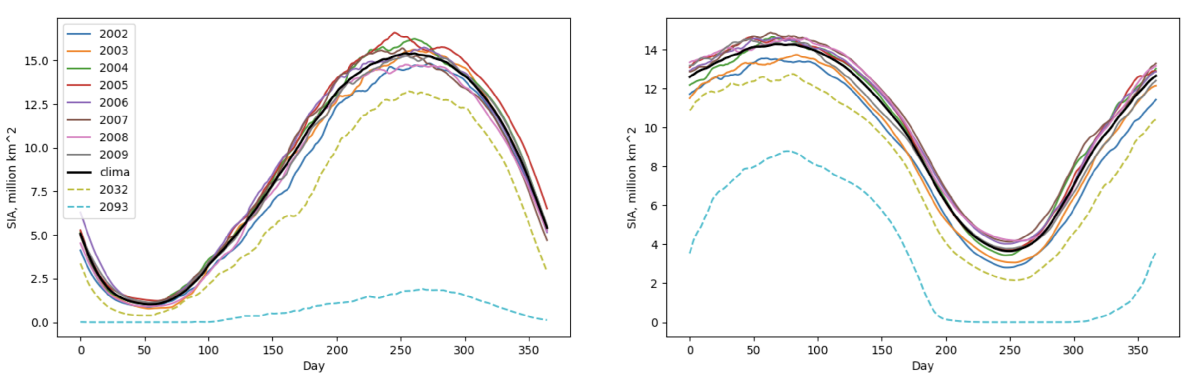

Figure S6: Seasonal evolution of sea ice area in Southern Ocean (left), Arctic Ocean (right) for individual years from 2002-2009, climatology and for future snapshot simulation for years 2032 and 2093.

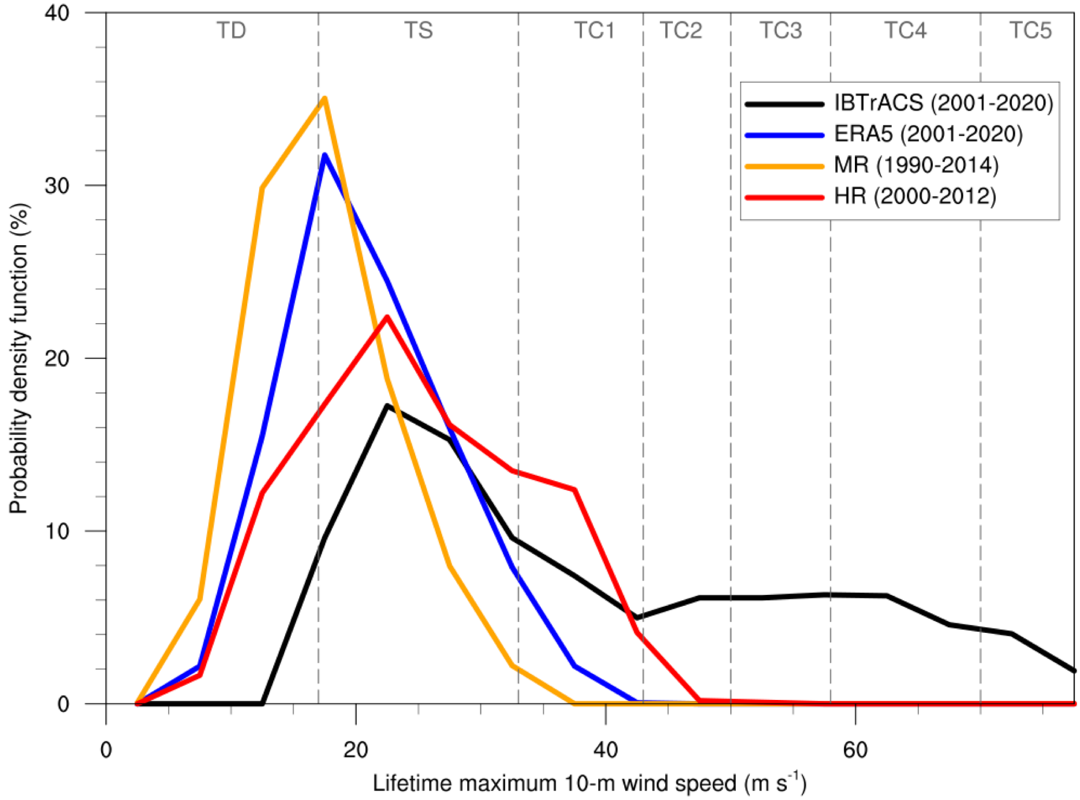

Figure S7: Probability distribution of present-day lifetime maximum 10 m wind speed (ms^{-1}) for tropical cyclones, detected using the OWPZ tracking scheme (see methods in Supplementary S1 and S2) for AWI-CM3 MR and HR simulations. Observation data is obtained from the International Best Track Archive for Climate Stewardship (IBTrACS) best track database version 4 (Knapp et al., 2010).

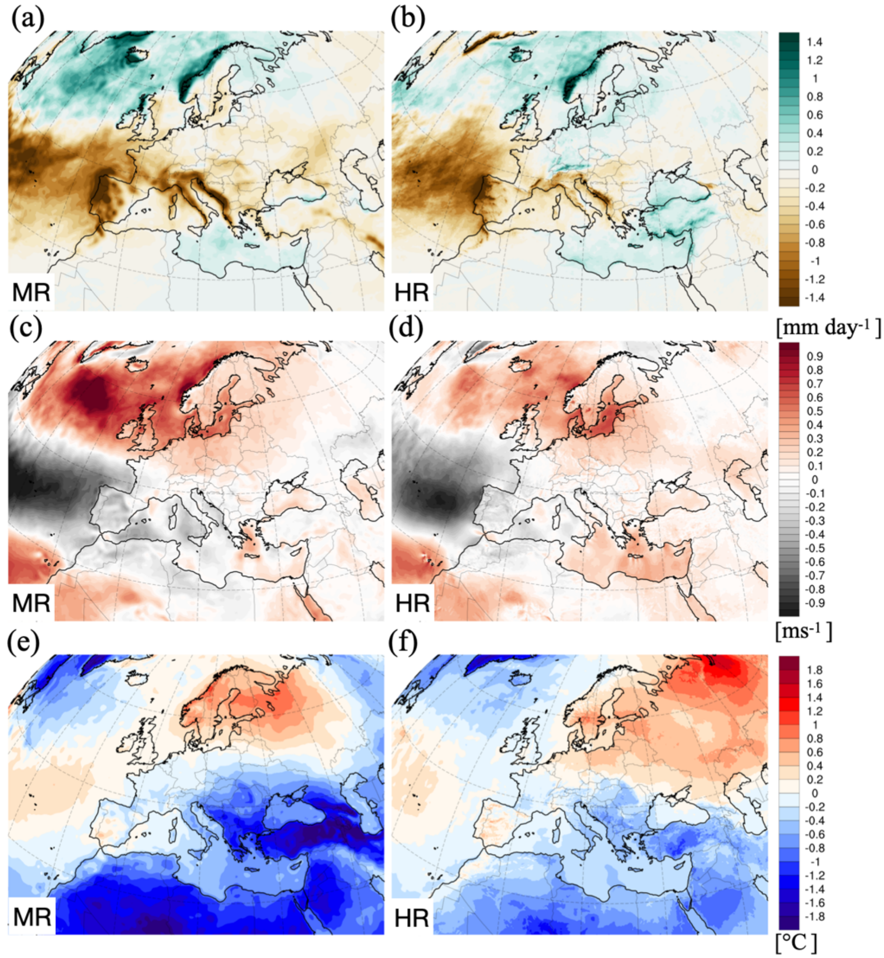

Figure S8: Precipitation (mmday^{-1}) regression with North Atlantic Oscillation Index using 15 years of the MR simulation (2085-2099) (a) and HR simulation (2090-2099 and 2090-2094) (b). (c) and (d), same as (a) and (b), but for the wind speed (ms^{-1}). (e) and (f), same as (a) and (b), but for the surface temperature (°C). The NAO index is based on the leading empirical orthogonal function of DJF seasonal mean sea level pressure anomalies over the North Atlantic and is normalized.

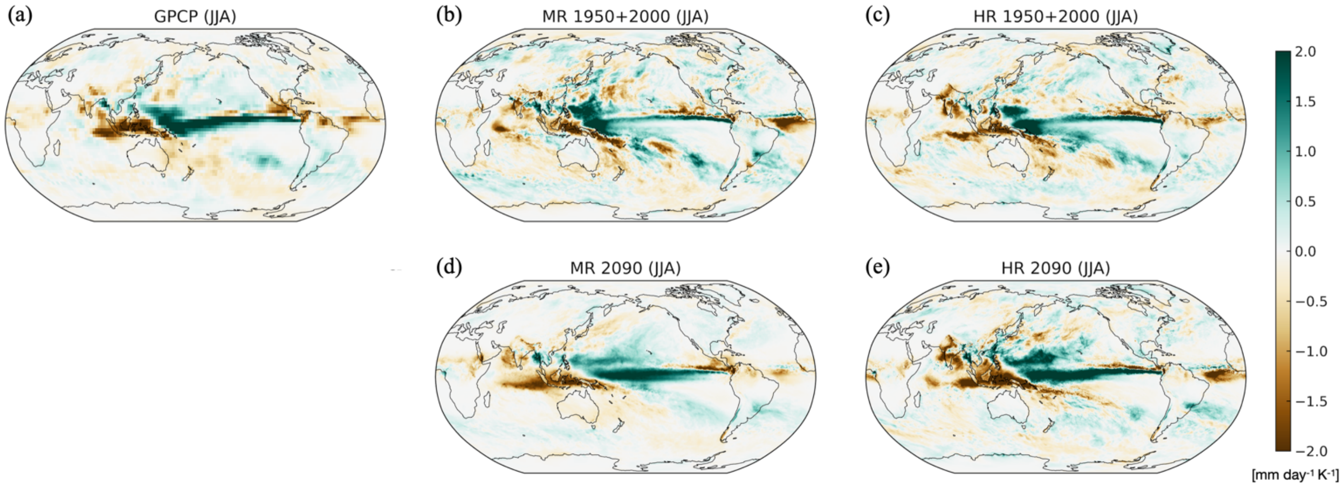

Figure S9: Regression between observed JJA Niño 3.4 SST anomalies and (a) observed rainfall (GPCP); (b) same as (a), but for MR (32 years of present-day climate); (c), same as (a), but for HR (32 years of present-day climate); (d), same (a)(b), but for 2090-2099 period (10+5 years); (e), same as (c), but for 2090-2099 period (10+5 years).

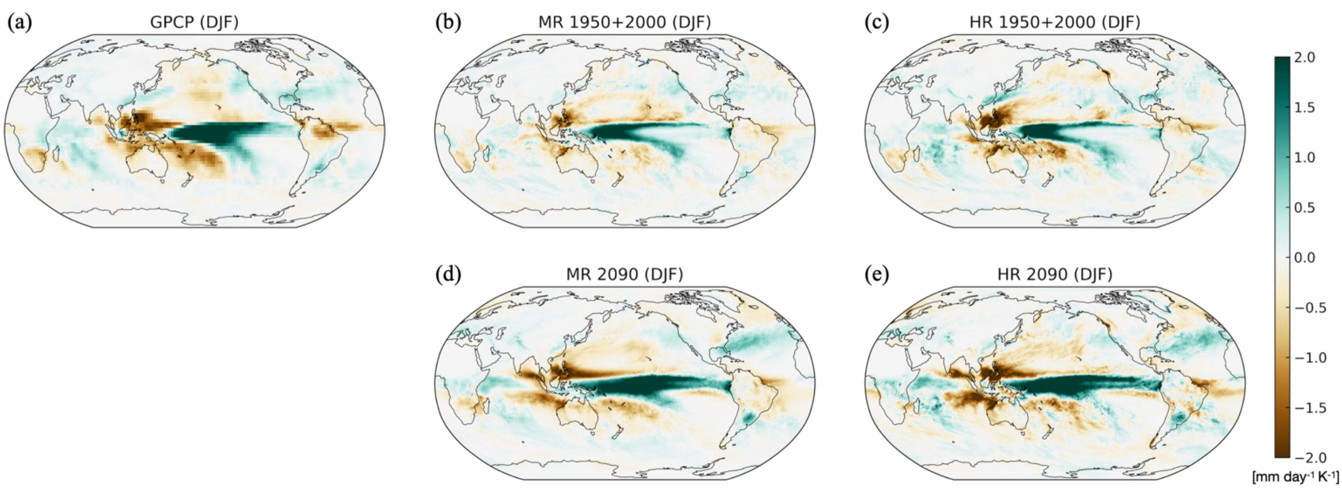

Figure S10: Regression between observed DJF Niño 3.4 SST anomalies and (a) observed rainfall (GPCP); (b) same as (a), but for MR (32 years of present-day climate); (c), same as (a), but for HR (32 years of present-day climate); (d), same (a)(b), but for 2090-2099 period (10+5 years); (e), same as (c), but for 2090-2099 period (10+5 years).

References

Kato, S., Rose, F. G., Rutan, D. A., Thorsen, T. J., Loeb, N. G., Doelling, D. R., Huang, X. L., Smith, W. L., Su, W. Y., and Ham, S. H.: Surface Irradiances of Edition 4.0 Clouds and the Earth's Radiant Energy System (CERES) Energy Balanced and Filled (EBAF) Data Product, J. Climate, 31, 4501-4527, https://doi.org/10.1175/jcli-d-17-0523.1, 2018.

Knapp, K. R., Kruk, M. C., Levinson, D. H., Diamond, H. J., and Neumann, C. J.: THE INTERNATIONAL BEST TRACK ARCHIVE FOR CLIMATE STEWARDSHIP (IBTrACS) Unifying Tropical Cyclone Data, B. Am. Meteorol. Soc., 91, 363-376, https://doi.org/10.1175/2009bams2755.1, 2010.

Raavi, P. H., Chu, J. E., Timmermann, A., Lee, S. S., and Walsh, K. J. E.: Moisture control of tropical cyclones in high-resolution simulations of paleoclimate and future climate, Nat. Commun., 14, 6426, https://doi.org/10.1038/s41467-023-42033-8, 2023.

Steele, M., Morley, R., and Ermold, W.: PHC: A global ocean hydrography with a high-quality Arctic Ocean, J. Climate, 14, 2079-2087, https://doi.org/10.1175/1520-0442(2001)014<2079:pagohw>2.0.co;2, 2001.

Tory, K. J., Chand, S. S., Dare, R. A., and McBride, J. L.: An Assessment of a Model-, Grid-, and Basin-Independent Tropical Cyclone Detection Scheme in Selected CMIP3 Global Climate Models, J. Climate, 26, 5508-5522, https://doi.org/10.1175/jcli-d-12-00511.1, 2013a.

Tory, K. J., Chand, S. S., Dare, R. A., and McBride, J. L.: The Development and Assessment of a Model-, Grid-, and Basin-Independent Tropical Cyclone Detection Scheme, J. Climate, 26, 5493-5507, https://doi.org/10.1175/jcli-d-12-00510.1, 2013b.